Dependence of the Scrape-Off Layer heat flux widths on external parameters in the NSTX

T.K. Gray[1], R. Maingi[1], J-W Ahn[1], A.G. McLean[1]
[1]*Oak Ridge National Laboratory, Oak Ridge TN USA*

1. Introduction

Spherical tori (ST) face the prospect of high heat flux onto the plasma facing components (PFC), owing to their compact nature and design as high power density systems. Power balance mandates a straightforward relationship between the peak heat flux and its characteristic footprint. The divertor heat flux profile and its characteristic scale length, λ_q are determined by the balance of parallel and radial thermal transport in the scrape-off layer (SOL), along with volumetric losses on the open field lines. Clearly λ_q is related to the upstream mid-plane density and temperature widths. Previously, National Spherical Torus Experiment [1] has performed scaling experiments to determine the dependence of the peak heat flux on controllable engineering parameters such as plasma current, heating power[2][3] and magnetic flux expansion [1]; in those experiments, a preliminary assessment of the divertor footprint was made. Understanding how those quantities scale [4] is a necessity for building larger, higher power spherical tori. The proposed NSTX-upgrade will stress the thermal limits of the existing graphite plasma facing components, with 10-12 MW of neutral beam input power, up to 6 MW of RF heating power, toroidal magnetic field up to 1T and plasma current of up to 2 MA with pulse lengths up to 5 sec [5]. Viable divertor designs may therefore require some form of heat flux mitigation techniques, including a detached or radiative divertor, magnetic flux expansion [6][7], and/or a snowflake divertor [8][9].

2. Experimental Set-up

NSTX is a medium size spherical torus with a major radius of 0.85 m and a minor radius $\leq$ 0.65 m (A $\geq$1.27). Plasma currents range from 0.6–1.4 MA, with toroidal magnetic fields in the range of 0.3–0.55 T and discharge lengths of $\leq$ 1.8s. Plasma heating is achieved by neutral beam injection typically ranging from 1–6 MW with core electron temperatures, $T_e(0) \simeq 0.6$–1.5 keV, and line-average electron densities, $n_e \simeq 1$–$6(10)^{19}$ m^{-3} . The NSTX divertor has an open geometry and as such is capable of a wide range of discharge shapes.

Surface infrared emissivity measurements are captured an Indigo Omega IR camera at a 30 Hz frame rate with surface temperature derived from both an *ex-situ* calibration with a blackbody calibration source as well as an *in-situ* calibration during vacuum bake-outs [2]. Since 2006 NSTX has employed evaporative lithium wall conditioning of its ATJ graphite plasma facing surfaces during some or all of the run campaign [10]. The data presented here are for discharges with boronized walls and not with lithium wall conditioning. This is because of the uncertainty the application of thin lithium coatings have on the surface emissivity of graphite tiles and how that emissivity is modified transiently during a discharge.

3. Results

Given the time resolution of the infrared camera system, measurements obtained are averaged over small edge localized modes (ELMs), although care is taken to filter out time slices just after large transients, disruptions or large ELMs that result in a large decrease in the plasma stored energy. In order to compare results from NSTX to those of other tokamaks, an integral definition of the characteristic scale length, $\lambda^{div}_{q,\,int}$ of the heat flux is used. This characteristic width was discussed in [11]:

$$\lambda_q^{div} \equiv \frac{P_{div}^{out}}{2\pi R_{div,\,peak}^{out}\, q_{div,\,peak}^{out}}, \qquad (1)$$

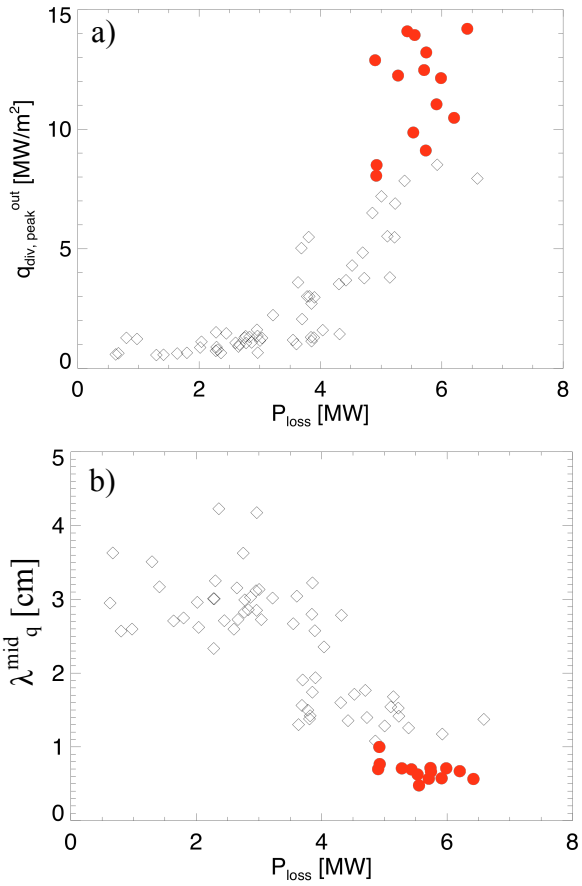

Figure 2: Scan of power lost through the last closed flux surface, P_{loss} for low triangularity (◊) and high triangularity (•) discharges. (a) Divertor heat increasing as P_{loss} increases. (b) Reduction in λ_q^{mid} as increase was a change in slope at approximately 4 MW suggesting a change in divertor regimes from detached/radiative to attached.

where $q^{out}_{div,\,peak}$ is the peak in the radial divertor heat flux measured from IR thermography, $R^{out}_{div,\,peak}$ is the radial location the peak heat flux occurs, and P^{out}_{div} is the outer divertor power derived from the measured divertor heat flux defined as,

$$P^{out}_{div} = \int_{R_{min}}^{R_{max}} 2\pi R^{out}_{div}\, q^{out}_{div}\, dr. \qquad (2)$$

The integral scale length, which will be referred to simply as λ_q^{div} for the remainder of this discussion, is then magnetically mapped to the mid-plane such that $\lambda_q^{mid} = \lambda_q^{mid} / f_{exp}$, where f_{exp} is the average magnetic flux expansion measured at the outer strike point along the ~ 5 mm midplane flux surface, and defined as $f_{exp} = \left(R_{mid} B_\theta^{mid}\right) / \left(R_{div} B_\theta^{div}\right)$. B_θ^{mid} and B_θ^{div} are the midplane and divertor poloidal magnetic fields at radial locations R_{mid} and R_{div} respectively. Note that the definition of λ_q^{div} used differs from previous analysis [2][3] where the scale length was quantified as either the full-width, half-maximum (FWHM) of the peak in the heat flux radial profile, $\lambda^{div}_{q,\,FWHM}$ or the exponential decay length of the SOL side of the profile, $\lambda^{div}_{q,\,exp}$. However, the integral method implicitly captures the magnitude and distribution of the divertor power better than the FWHM or exponential definitions, and allows for variations in flux expansion, thus allowing for better cross-machine comparisons [11].

3.1 λ_q^{mid} *scaling with* P_{loss} -- Figure 2 shows that as P_{loss}, which is defined as the power flowing through the last closed flux surface or $P_{loss} = P_{NBI} + P_{oh} - dW/dt - P^{core}_{rad}$, is increased from 0.5 to 6 MW the heat flux increases as expected. Previous scaling results [3] reported similar trends as shown in Fig. 2(b), but λ_q^{div} was defined in terms of the full-width, half-maximum of the heat flux profile. Note that the heat flux width, λ_q^{mid} shown in Fig. 2(b) follows the integral λ_q^{mid} defined in Eq. 2. For low triangularity discharges ($\delta \sim 0.5$), there is a step-discontinuity in λ_q^{mid} as P_{loss} is increased beyond ~ 4 MW, shifting from an average λ_q^{mid} of approximately 3 cm down to 1.25 cm. This is due to a transition from a radiative (or possibly detached) divertor to an attached divertor at P_{loss} = 4 MW, the radiated power drops as P_{loss} is increased [12] and is consistent with the 2-point modeling [3][13]. We note, however, that a detailed analysis of the divertor regime [14] to detect whether detachment itself and volume recombination is occurring in the divertor region has yet to be performed.

For the high triangularity discharges shown in Fig. 2(b), where $\delta \sim 0.7$, $f_{exp} = 16$ and $I_p = 1.2$ MA, λ_q^{mid} is constant at ~0.7 cm. However, these data for high triangularity discharges were limited to $P_{loss} \geq 5$ MW. Therefore, λ_q^{mid} appears to vary weakly with P_{loss}, especially when the divertor is in an attached regime. We will show in the next section that this difference in λ_q^{mid} values at low and high triangularity are actually due to a strong I_p dependence.

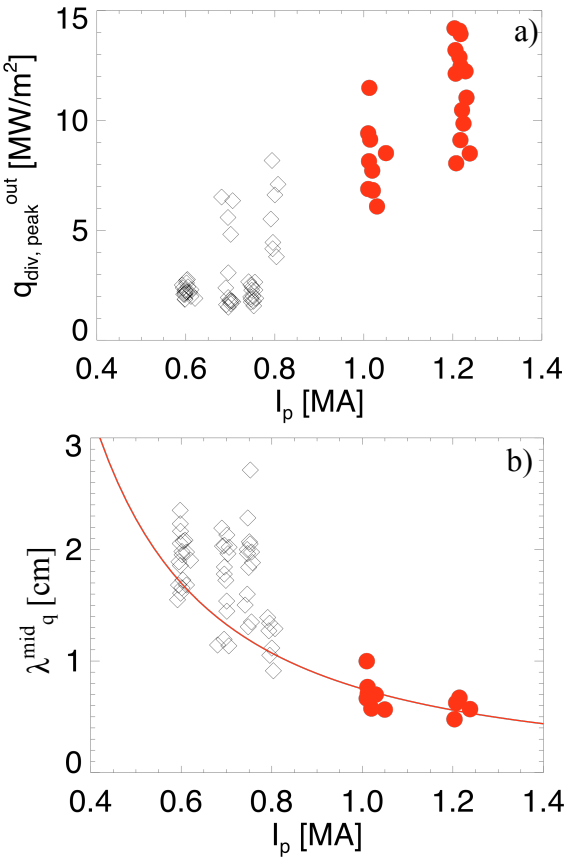

Figure 3: Effect of increasing plasma current, I_p for low triangularity (◊) and high triangularity (•) discharges. (a) Divertor heat flux increases with increasing plasma current. (b) λ_q^{mid} contracts with increasing plasma current. (—) Power law fit to the λ_q^{mid} data.

3.2 *λ_q^{mid} scaling with plasma current* -- Since the results of the previous two sections showed λ_q^{mid} is largely independent of flux expansion and P_{loss}, data from a number of discharges have been used to determine of the heat flux and λ_q^{mid} scale as a function of plasma current. This is shown in Fig. 3 for low triangularity discharges ($\delta \sim 0.5$) where 4 MW of beam power and a narrow flux expansion of 6 were used, as well as high triangularity discharges ($\delta \sim 0.7$) with a much higher flux expansion of 16 and a beam heating power of 6 MW. The trends shown are therefore indicative of the wide range of plasma parameters used; however, although λ_q^{mid} has shown minimal dependencies on other parameters, these dependences have probably resulted in the scatter in part of the data shown in Fig. 2.

From Fig. 3(b), λ_q^{mid} is seen to strongly contract with increasing plasma current. From the data presented in Fig. 3(b), it can be shown that the heat flux width scales with the plasma current as $\lambda_q^{mid} = 0.91 I_p^{-1.62}$. It should be noted that both DIII-D [15] and JET [16] have reported that $\lambda_q^{mid} \sim 1/I_p$, i.e. a somewhat weaker dependence but in the same direction. The NSTX results are applicable over the large range of the plasma shape, flux expansion, q_{95} and heating power of the discharges used in the dataset. Understanding why λ_q^{mid} contracts with increasing plasma current is the subject of ongoing investigation.

Recent simulations with the SOLT code [17], which simulates midplane SOL turbulence, were able to describe trends λ_q^{mid} observed in low power, ELM-free H-mode discharges. However, similar agreement between measured and simulated λ_q^{mid} was not possible for the plasma current scaling seen in high power, H-mode NSTX discharges. This suggests that midplane turbulence is not the underlying cause of the contraction in λ_q^{mid} with respect to I_p but that some other mechanism that is not included in SOLT such as divertor leg instabilities [18], hot ion losses or MHD activity that moves the strike point is the underlying cause of the contraction in λ_q^{mid}.

Summary and Conclusions

By magnetically mapping the divertor scale length, λ_q^{div} to the midplane, we have determined that the footprint depends at most weakly with plasma heating power and flux expansion. This yields a simple relation for the mid-plane heat flux width with respect to the plasma current, where λ_q^{mid} is shown to contract strongly with plasma current such that $\lambda_q^{mid} = 0.91 I_p^{-1.62}$. This scaling covers a wide range of plasma shapes, flux expansions and heating powers. Future experiments planned to further explore the density dependence of λ_q^{mid} as well as the effect of lithium wall conditioning using a 2-color IR diagnostic recently developed [19] that should be less susceptible to emissivity changes on the divertor tiles.

To estimate what can be expected for NSTX-Upgrade, Eq. 1 can be re-written to estimate the peak heat flux on the divertor such that $q_{div,peak}^{out} = P_{div}^{out} / \left(2\pi R_{div,peak}^{out} f_{exp} \lambda_q^{mid}\right)$, where $P_{div}^{out} \approx f_{div} P_{heat}$, $f_{div} = 0.5$ and λ_q^{mid} can be treated as a known function of I_p. Therefore, for operating conditions of I_p = 2 MA and P_{NBI} = 12 MW, which are the maximum design points of NSTX-U, then the peak heat flux to the divertor would reach 24 ± 4 MW/m^2 for $\delta \sim 0.7$ and $f_{exp} = 30$. This calculation does not take credit for any method of heat flux mitigation such as a radiative or detached divertor. It is thus clear that some technique or combination of techniques of heat flux mitigation will be required for NSTX-U. Therefore, given the potentially large magnitudes of divertor heat fluxes expected, fully understanding λ_q^{mid}'s strong dependence on plasma current is a necessity for a next step ST, and the focus of near term theoretical modeling.

Acknowledgements

The authors are grateful to the NSTX research team for diagnostic and technical support. T.K. Gray is supported under an appointment to the U.S. D.O.E. Fusion Energy Postdoctoral Research Program administered by the Oak Ridge Institute for Science and Education under contract number DE-AC05-06OR23100 between the U.S. D.O.E. and Oak Ridge Associated Universities. This research is sponsored by US DOE contracts DE-AC05-00OR22725, DE-AC52-07NA27344, and DE-AC02-09CH11466.

References

[1] M. Ono et al. Nucl. Fusion **40** (2000) 557-561.
[2] R. Maingi et al. J. Nucl, Mater. **313-316** (2003) 1005-1009
[3] R. Maingi et al. J. Nucl. Mater. **363–365** (2007) 196–200.
[4] T.K. Gray, et al. Submitted to J. Nucl. Mater.
[5] J.E. Menard, et al. These Proceedings
[6] V.A. Soukhanovskii, et al. Nucl. Fusion **49** (2009) 095025
[7] V.A. Soukhanovskii, et al. Phys. Plasmas **16** (2009) 022501
[8] D.D. Ryutov Phys. Plasmas **14** (2007) 064502
[9] V.A. Soukhanovskii, et al. submitted to J. Nucl. Mater.
[10] H.W. Kugel et al. Phys. Plasmas. **15** (2008) 056118.
[11] A. Loarte et al. J. Nucl. Mater. **266-269** (1999) 587–592.
[12] S.F. Paul et al. J. Nucl. Mater. **337–339** (2005) 251–255.
[13] K. Borass et al. Nucl. Fusion **31** (1991) 1035.
[14] V.A. Soukhanovskii et al. J. Nucl. Mater. **337–339** (2005) 475–479.
[15] C.J. Lasnier, et al. submitted to J. Nucl. Mater (2010)
[16] W. Fundamenski, Private Communication (2009)
[17] J.R. Myra et al. submitted to J. Nucl. Mater (2010)
[18] R.H. Cohen et al. Nucl. Fusion **47** (2007) 612-625.
[19] A.G. McLean et al. submitted to Rev. Sci. Instrum. (2010)